chemosensors

MDPI

Article

Excellent Cooperation between Carboxyl-Substituted Porphyrins, k-Carrageenan and AuNPs for Extended Application in CO_2 Capture and Manganese Ion Detection

Camelia Epuran [1], Ion Fratilescu [1], Ana-Maria Macsim [2], Anca Lascu [1], Catalin Ianasi [1], Mihaela Birdeanu [3] and Eugenia Fagadar-Cosma [1,*]

[1] Institute of Chemistry "Coriolan Dragulescu", Mihai Viteazu Ave. 24, 300223 Timisoara, Romania; ecamelia@acad-icht.tm.edu.ro (C.E.); ionfratilescu@acad-icht.tm.edu.ro (I.F.); alascu@acad-icht.tm.edu.ro (A.L.); ianasic@acad-icht.tm.edu.ro (C.I.)
[2] Institute of Macromolecular Chemistry "Petru Poni", Grigore Ghica Vodă Alley, No. 41A, 700487 Iasi, Romania; macsim.ana@icmpp.ro
[3] National Institute for Research and Development in Electrochemistry and Condensed Matter, Plautius Andronescu Street 1, 300224 Timisoara, Romania; mihaelabirdeanu@gmail.com
* Correspondence: efagadar@yahoo.com or efagadarcosma@acad-icht.tm.edu.ro

Abstract: Significant tasks of the presented research are the development of multifunctional materials capable both to detect/capture carbon dioxide and to monitor toxic metal ions from waters, thus contributing to maintaining a sustainable and clean environment. The purpose of this work was to synthesize, characterize (NMR, FT-IR, UV-Vis, Fluorescence, AFM) and exploit the optical and emission properties of a carboxyl-substituted A_3B porphyrin, 5-(4-carboxy-phenyl)-10,15,20-tris-(4-methyl-phenyl)–porphyrin, and based on it, to develop novel composite material able to adsorb carbon dioxide. This porphyrin-k-carrageenan composite material can capture CO_2 in ambient conditions with a performance of 6.97 mmol/1 g adsorbent. Another aim of our research was to extend this porphyrin- k-carrageenan material's functionality toward Mn^{2+} detection from polluted waters and from medical samples, relying on its synergistic partnership with gold nanoparticles (AuNPs). The plasmonic porphyrin-k-carrageenan-AuNPs material detected Mn^{2+} in the range of concentration of 4.56×10^{-5} M to 9.39×10^{-5} M (5–11 mg/L), which can be useful for monitoring health of humans exposed to polluted water sources or those who ingested high dietary manganese.

Keywords: carboxyl-substituted A_3B porphyrin; NMR; UV-Vis; fluorescence; porphyrin-k-carrageenan composite material; plasmonic porphyrin-k-carrageenan-AuNPs material; CO_2 capturing; Mn^{2+} detection

check for updates

Citation: Epuran, C.; Fratilescu, I.; Macsim, A.-M.; Lascu, A.; Ianasi, C.; Birdeanu, M.; Fagadar-Cosma, E. Excellent Cooperation between Carboxyl-Substituted Porphyrins, k-Carrageenan and AuNPs for Extended Application in CO_2 Capture and Manganese Ion Detection. *Chemosensors* **2022**, *10*, 133. https://doi.org/10.3390/chemosensors10040133

Academic Editor: Kien Wen Sun

Received: 9 March 2022
Accepted: 30 March 2022
Published: 1 April 2022

Publisher's Note: MDPI stays neutral with regard to jurisdictional claims in published maps and institutional affiliations.

Copyright: © 2022 by the authors. Licensee MDPI, Basel, Switzerland. This article is an open access article distributed under the terms and conditions of the Creative Commons Attribution (CC BY) license (https://creativecommons.org/licenses/by/4.0/).

1. Introduction

The capture of carbon dioxide into appropriate adsorbent materials represents an actual scientific task since the accumulation of greenhouse gas is associated with an undesired increase in temperature all around the world. For this purpose, a large variety of materials based on porphyrins was investigated, among which a series of porous hexanuclear rare-earth metal–organic frameworks (MOFs) based on Ce(III) salts and 5,10,15,20-tetrakis(4-carboxy-phenyl)-porphyrin exhibited excellent CO_2 adsorption properties up to 42.4 cm^3 (83.2 mg)/g at 273 K and normal pressure [1]. A new two-dimensional covalent organic framework based on 5,10,15,20-tetra-(4-amino-phenyl)-porphyrin and 1,1′,2,2′-tetrakis-(4-formyl-(1,1′-biphenyl) ethene was used as gas storage material with a greater capacity for CO_2 adsorption of 187 mg/g, but came with the disadvantage of needing higher pressure and temperature (50 bar and 323 K) [2].

Zinc-tetraphenylporphyrin solubilized by means of a protein cage from *E. coli* (30 porphyrins per protein cage) was also used for CO_2 capture [3]. In addition, the protein-caged porphyrin is able to catalyze the CO_2 transformation into $CaCO_3$, even at

60 °C, and no side reactions have been detected [4]. The capture and catalytic conversion of CO_2 into cyclic carbonates could be also obtained on a Co(II)-porphyrin-covalent-organic framework using cobalt(II)-5,10,15,20-tetrakis(4-amino-phenyl)-porphyrin building block and 1,3,6,8-tetrakis(4-formyl-phenyl)pyrene [5]. The best CO_2 adsorption capacity of these nanomaterials was 169 mg/g at 298 K and the yield in cyclic carbonates was 92% under mild conditions (at 313 K and 0.1 MPa).

Other attempts to transform CO_2 were based on its electrochemical reduction performed on a graphite electrode coated via electrochemical polymerization with thiophene-functionalized Co(II)-porphyrin, as mediator/catalyst [6].

Our group's experience regarding the detection and capturing of carbon dioxide by means of using porphyrin-based functionalized materials is reflected in the numerous published papers. Thus, multifunctional materials containing 5-(4-carboxy-phenyl)-5,10,15-tris(4-phenoxy-phenyl)-porphyrin, iron oxide magnetic nanoparticles (MNPs), a polysaccharide, k-carrageenan and a silica linker, were tested both as catalysts for the Knoevenagel condensation of aldehydes at room temperature and for the capacity to detect CO_2. The concentration range of CO_2 detection spans from 30 μM to 200 μM [7]. Other types of hybrid materials were obtained by incorporation into tetra-ethyl-orthosilicate (TEOS)-based silica matrices of either Pt(II)-5,10,15,20-tetra-(4-allyloxy-phenyl)-porphyrin (PtTAOPP) or platinum nanoparticles (PtNPs), or in tandem with 5,10,15,20-tetra-(4-allyloxy-phenyl)-porphyrin (TAOPP). Among these, (PtTAOPP)-silica hybrid was the most efficient material for CO_2 adsorption (25 mmol/g) under normal conditions [8], the second-best world known performance, with the first being 44.2 mmol/g amount of CO_2 at 373 K and 10 bar [9]. Pyridyl substituted porphyrins, such as 5-(4-pyridyl)-10,15,20-tris(3,4-dimethoxy-phenyl)-porphyrin, proved to be useful for CO_2 detection in space habitable areas [10]; another A_3B derivative, 5-(4-pyridyl)-10,15,20-tris(4-phenoxy-phenyl)-porphyrin, incorporated into a biocompatible polymer, polyvinylpyrrolidone, was successful both in optical and colorimetric sensing for monitoring CO_2, in the concentration range 45–150 μmol/L [11], which is useful for monitoring CO_2 level in baby's nursery.

The main purpose of this work was to develop a new kind of composite material that was able to capture carbon dioxide based on an organic nontoxic polymer, k-carrageenan [12–15], and a carboxyl-substituted porphyrin, 5-(4-carboxy-phenyl)-10,15,20-tris-(4-methyl-phenyl)-porphyrin (Figure 1).

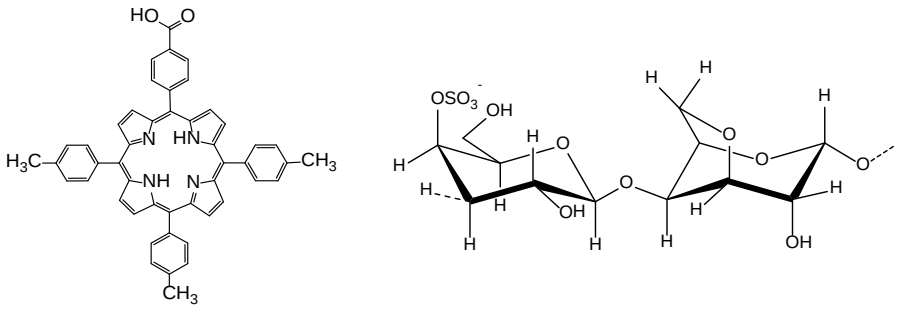


Figure 1. Structures of 5-(4-carboxyphenyl)-10,15,20-tris-(4-methyl-phenyl)-porphyrin (5-COOH-3MPP) (**a**) and of k-carrageenan (**b**).

The second aim was to extend this porphyrin-based material functionality toward ion metal detection based on its synergistic approach with gold nanoparticles (AuNPs). The plasmonic material, porphyrin-k-carrageenan-AuNPs, was designed with the purpose to detect Mn^{2+} from polluted waters or medical samples.

Monitoring manganese is a demand because chronic Mn^{2+} intoxication leads to Parkinson-like neurodegenerative disorder known as manganism, inducing basal ganglia atrophy in humans [16], a disease that is usually encountered by miners, welders and steel and battery workers. Manganism, which is considered endemic in some South African

manganese mines, might be associated with nerve toxicity, producing anxiety, dementia, ataxia and a 'mask-like' face [17,18]. For example, the European Commission and the United States Environmental Protection Agency have set the Mn^{2+} level in drinking water at 0.05 mg/L. In China, the maximum level in surface water is 0.1 and 5.0 mg/L in wastewater [17]. The normal Mn^{2+} concentrations in blood range from 4 to 15 µg/L in humans [19]. The average manganese concentration of untreated mine waters is around 17.7 mg/L at surfaces mines [20]. Therefore, Mn^{2+} monitoring from wastewater is demanded to reduce the negative impacts on both the aqueous environment and human health. Although health standards limit the Mn concentration in drinking water to 0.4 mg/L this value is 20 times lower than the effluent standard of Japan (10 mg/L) [21].

Porphyrin-bases are well-known to be capable to detect metal ions or metal nanoparticles spectroscopically. This property was exploited by 5-(4-carboxy-phenyl)-10,15,20-triphenyl-porphyrin for the detection of Ag^0 (2.50×10^{-9} M to 0.82×10^{-7} M) [22] and for Pt^0 recovery in the concentration interval 2.77 to 40.45×10^{-6} M using 5,10,15,20-tetrakis(4-amino-phenyl)-porphyrin, respectively [23]. Potentiometric method was extensively used to detect metal ions (Cr^{3+}, Cu^{2+}, Fe^{3+}), using as sensitive materials various porphyrin derivatives incorporated into polymeric matrices [24–26].

2. Materials and Methods

2.1. Materials

Methyl 4-formylbenzoate and 4-methylbenzaldehyde (*p*-tolualdehyde) were acquired from Aldrich, St. Louis; pyrrole, propionic acid, propionic anhydride, hexane and silica gel from Scharlab (0.04–0.06 mm, 230–400 mesh); sodium citrate, DMF, $MnCl_2$, $FeCl_3$ and KCl originated from Merck; dichloromethane THF Supelco production; KOH was purchased from Lachema; ethanol was received from Tunic, Romania; HCl 37%, Na_2CO_3 and $MgSO_4$ came from Chimopar Romania; Na_2SO_4 and $CaCl_2$ from Chimreactiv Romania; k-carrageenan and $HAuCl_4 \times 3H_2O$ were supplied by Roth, Karlsruhe; $CuCl_2$, $FeSO_4$, NaCl, $ZnCl_2$ and $Pb(NO_3)_2$ were produced by Reactivul Bucuresti.

2.2. Apparatus

The emission spectra were registered on a Perkin-Elmer Model LS 55 apparatus (PerkinElmer, Inc./UK Model LS 55, Waltham, MA, USA), using 1 cm path length cells, excitation slits of 10 nm and emission slits of 6 nm, at ambient temperature (22−24 °C), without cut-off filters, λ_{ex} = 432 nm. The UV-Vis spectra were recorded on a V-650-JASCO spectrometer (Pfungstadt, Germany) using 1 cm optical path length. The pH values were measured with a pH-meter HI 98,100 Checker Plus, from Hanna Instruments (Woonsocket, RI, USA). The Rota-evaporator was from Heidolph Laborota 4010 digitally equipped with the vacuum pump PC 610 CVC2, Vacuumbrand GmbH. The atomic force microscopy (AFM) images were obtained on a Nanosurf® EasyScan 2 Advanced Research AFM microscope (Liestal, Switzerland) equipped with a piezoelectric ceramic cantilever. Pure silica plates were used for the deposition of samples. FT-IR spectra were recorded on a JASCO 430 FT-IR (Hachioji, Tokyo, Japan) spectrometer from KBr pellets in the range 4000–400 cm^{-1}. The ^{1}H-NMR and ^{13}C-NMR spectra were registered on a Bruker Avance NEO Spectrometer at 400 MHz, equipped with 5 mm four nuclei (^{1}H/^{13}C/^{19}F/^{29}Si) direct detection probe (Rheinsteitten, Germany), in $CDCl_3$. The chemical shifts are expressed in (ppm), using as reference tetramethylsilane (TMS).

2.3. The Method for Obtaining of 5-(4-Methoxy-carbonyl-phenyl)-10,15,20-tris-(4-methyl-phenyl)-porphyrin (5-COOCH3-3MPP)

Porphyrin (5-COOCH3-3MPP) was obtained by multicomponent synthesis, presented in detail in Section 2.3 of the Supplementary Materials. The structures of the six different reaction products are illustrated in Figure S1, and the thin layer chromatography (TLC) using as eluent CH_2Cl_2 is represented in Figure S2.

2.4. Hydrolysis of Porphyrin Ester (5-COOCH3-3MPP) to 5-(4-Carboxy-phenyl)-10,15,20-tris-(4-methyl-phenyl)-porphyrin (5-COOH-3MPP)

The porphyrin ester (5-COOCH3-3MPP) was hydrolyzed to its COOH-porphyrin derivative in strong alkaline conditions (Figure 2) using a mixture of KOH and ethanol, as presented in Section 2.4 of the Supplementary Materials.

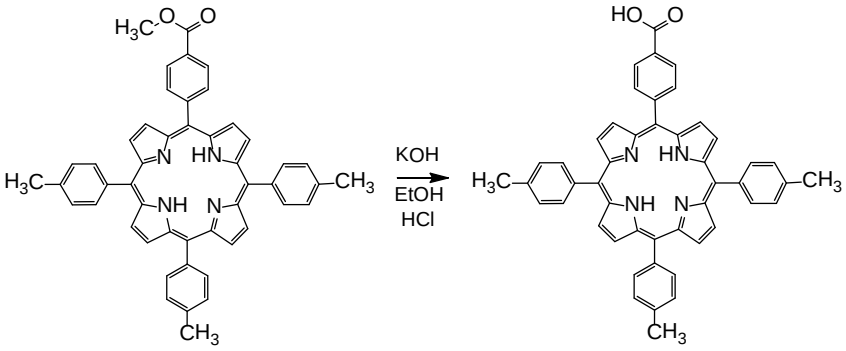


Figure 2. Hydrolysis reaction of porphyrin ester (5-COOCH3-3MPP) to carboxyl substituted derivative (5-COOH-3MPP).

2.5. Physical-Chemical Characterization of the Two Obtained Porphyrins

The UV-Vis (Figure S3), FT-IR (Figure S4), ^{1}H-NMR and ^{13}C-NMR (Figures S5–S7) spectra of (5-COOCH3-3MPP) and (5-COOH-3MPP) are discussed in detail in the Supplementary Materials (Sections 2.5.1–2.5.3).

The main physical characteristics of (5-COOCH3-3MPP) porphyrin: 5-(4-methoxycarbonyl-phenyl)-10,15,20-tris-(4-methyl-phenyl)-porphyrin are: violet crystals; yield 15%, m.p. over 320 °C; ^{1}H-NMR ($CDCl_3$, 400 MHz), δ, ppm: 8.918–8.794 (dd, 8H, *β*-pyrrole); 8.476–8.455 (d, 2H, *o*-phenyl from methyl-benzoate); 8.345–8.324 (d, 2H, *m*-phenyl from methyl-benzoate); 8.133–8.113 (d, 6H, *o*-phenyl from tolyl); 7.595–7.575 (d, 6H, *m*-phenyl from tolyl); 4.139 (s, 3H, -OCH_3); 2.734 (s, 9H, -CH_3); −2.746 (s, 2H, N*H*). ^{13}C-NMR ($CDCl_3$, 100 MHz), δ, ppm: 167.37 (O-*C*=O); 147.19 (*C*=N); 118.23 (O-*C*H_3); 21.51 (-*C*H_3). FT-IR (KBr), cm^{-1}: 3312 (ν_{N-H}); 2917 (ν_{C-H}); 1728 ($\nu_{C=O}$); 1604 ($\nu_{C=C}$); 1469 ($\nu_{C=N}$); 1272 (ν_{C-O-C}); 1183 ($\delta_{C-Hpyrrole}$); 965 (γ_{C-H}); 796 ($\gamma_{C-Hpyrrole}$). UV-Vis, THF (λ_{max} (logε)): 417 (5.61); 514 (4.32); 549 (4.04); 592 (3.80); 649 (3.78). Eluent: dichloromethane, Rf = 0.76.

Most important physical characteristics of (5-COOH-3MPP) porphyrin: 5-(4-carboxyphenyl)-10,15,20-tris-(4-methyl-phenyl)-porphyrin are: violet crystals; yield 85%, m.p. over 320 °C; ^{1}H-NMR ($CDCl_3$, 400 MHz), δ, ppm: 8.89–8.78 (dd, 6H, *β*-pyrrole); 8.712 (s, 2H, *β*-pyrrole); 8.493–8.479 (d, 2H, *o*-phenyl from -C_6H_5-COOH); 8.357–8.377 (d, 2H, *m*-phenyl from -C_6H_5-COOH); 8.119–8.091 (d, 6H, *o*-phenyl from tolyl); 7.574–7.555 (d, 6H, *m*-phenyl from tolyl); 2.712 (s, 9H, -CH_3); −2.771 (s, 2H, N*H*). FT- IR (KBr), cm^{-1}: 3312 (ν_{N-H}); 2919 (ν_{C-H}); 1686 ($\nu_{C=O}$); 1603 ($\nu_{C=C}$); 1466 ($\nu_{C=N}$); 1283 (ν_{C-O}); 1178 ($\delta_{C-Hpyrrole}$); 963 (γ_{C-H}); 794 ($\gamma_{C-Hpyrrole}$). UV-Vis, THF (λ_{max} (logε)): 417 (5.65); 514 (4.36); 549 (4.08); 593 (3.85); 649 (3.85).

3. Results

3.1. Method for Capturing CO_2 Gas by the (5-COOH-3MPP)-k-Carrageenan Composite Material, in DMF/Water Mixture

A volume of 3.9 mL of the gel was diluted with 62.4 mL mixture of DMF: water = 2:3. A change in color was observed from violet to violet-yellow. The adding of the DMF: water mixture led to a hypochromic effect regarding the Soret band, accompanied by bathochromic shifts for all the absorption bands (Figure 3), as follows: for the Soret band from 418 nm to 420 nm, for QIV band from 515 nm to 520 nm, for QIII band from 550 nm to 554 nm, for QII band from 592 nm to 594 nm and for QI from 548 nm to 651 nm, respectively.

The sol thus obtained was sealed in an Erlenmeyer flask equipped with a magnetic stirrer, an elastic rubber cork and three syringe needles: one for the bubbling of CO_2 gas,

one for maintaining pressure control and one for sampling (Figure S8-Supplementary Material). A constant flow rate of 10 mL/min of CO_2 gas was passed through the sol under constant stirring (1000 rpm), and samples were taken every 2 min for UV-Vis (Figure 4).

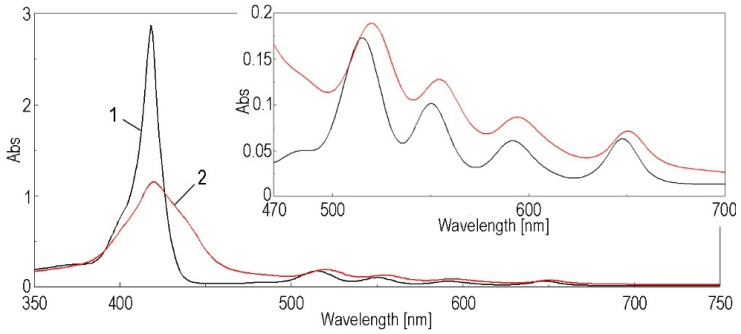


Figure 3. Overlapped UV-Vis spectra for the (5-COOH-3MPP)-k-carrageenan composite gel diluted with only DMF (1) and with DMF: water = 2:3 (*v*/*v*) mixture (2).

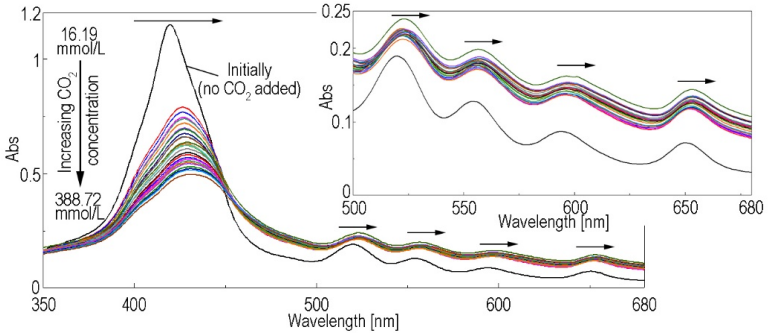


Figure 4. UV-Vis absorption spectra during CO_2 gas capture in the sol containing (5-COOH-3MPP)-k-carrageenan composite, in DMF:water = 2:3 (*v*/*v*) mixture.

It can be observed that the accumulation of CO_2 in the sol leads to the bathochromic shift of the absorption maxima and also to a hypochromic effect. This shift to longer wavelengths can be attributed to the slight protonation of the porphyrin molecules, as carbonic acid is accumulating in the mixture due to the presence of water in the system. The acid environment produced by adding CO_2, might favor the formation of J-type aggregates, also causing the enlargement of the Soret band [11]. An isosbestic point at 453 nm is observed, marking both the generation of protonated porphyrins and the link between CO_2 and the -NH from internal ring of porphyrins. Figure 5 represents the linear dependence of the intensity of absorption of (5-COOH-3MPP)-k-carrageenan composite read at 420 nm and the molar concentration of CO_2 gas in the sol.

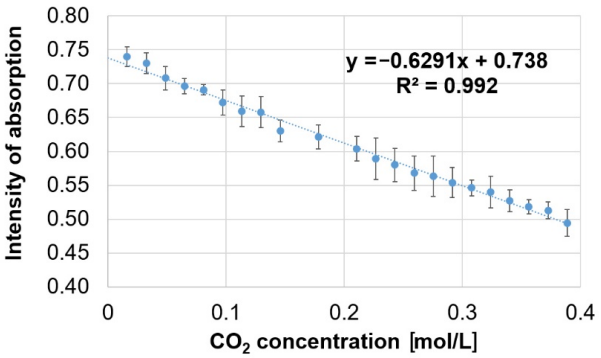


Figure 5. Linear dependence between the intensity of absorption of (5-COOH-3MPP)-k-carrageenan composite read at 420 nm and the concentration of CO_2 in the sol, realized during 60 min of CO_2 exposure, flow rate of 10 mL/min.

The same samples were subjected to fluorescence measurements, where it can be observed that the accumulation of carbon dioxide in the mixture leads to the quenching of the fluorescence (Figure 6). The (5-COOH-3MPP)-k-carrageenan composite emission intensity decreases in a linear fashion with the increase in CO_2 gas concentration. This linear dependence is characterized by a confidence coefficient of 99.33% (Figure 7).

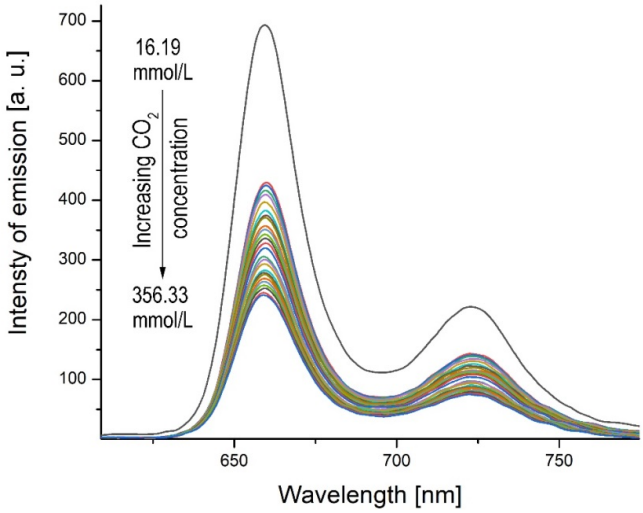


Figure 6. Overlapped emission spectra showing the quenching of the fluorescence due to interaction between (5-COOH-3MPP)-k-carrageenan and CO_2 gas, λex = 432 nm, excitation slit = 10 nm, emission slit = 7.5 nm and scan speed = 1200 nm/min.

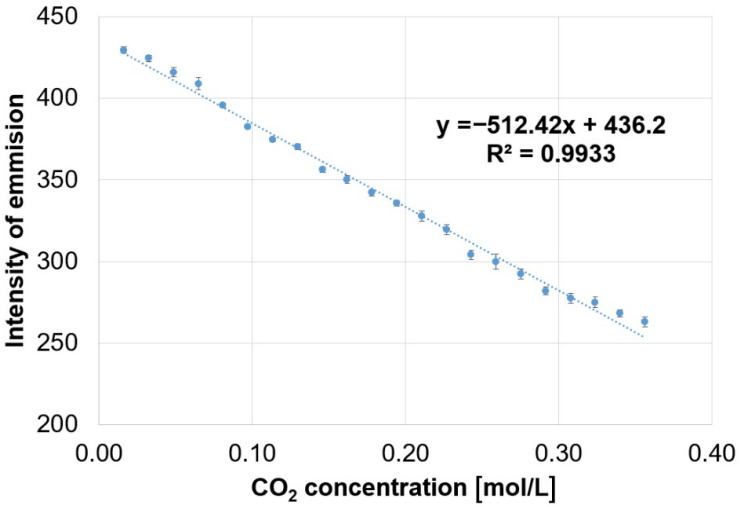


Figure 7. Linear dependence between the intensity of emission measured at 660 nm for the (5-COOH-3MPP)-k-carrageenan during 60 min of CO_2 gas exposure (flow rate of 10 mL/min).

A quantity of 1 g composite material that contains 0.09 g porphyrin can capture 6.97 mmol CO_2. This result is six times lower than the best-reported result [9], which is 42 mmol CO_2/1 g adsorbent material but obtained with the supplementary inconveniences of using high temperature and pressure of 373 K and 10 bar, respectively. The significant sustainability of our work is that this result has been obtained under normal conditions. Nevertheless, this result is among the best results reported in the literature in the last decade [1–5]. We presume that these polymer–porphyrin-based materials can be extended for the detection or monitoring of other gases requiring recovery or control [27].

AFM Investigation of the (5-COOH-3MPP) and (5-COOCH3-3MPP) Porphyrins and of the Composite Material (5-COOH-3MPP)-k-Carrageenan, before and after treatment with CO_2

The AFM image of 5-(4-methoxycarbonyl-phenyl)-10,15,20-tris-(4-methyl-phenyl)-porphyrin deposited from THF (Figure 8a) on silica plates reveals macaron-like aggregates (dome shaped) with diameters ranging from 610 to 736 nm, and a medium height of 140 nm, unevenly dispersed on the surface. They are the result of the H-type aggregation [28] of smaller particles.

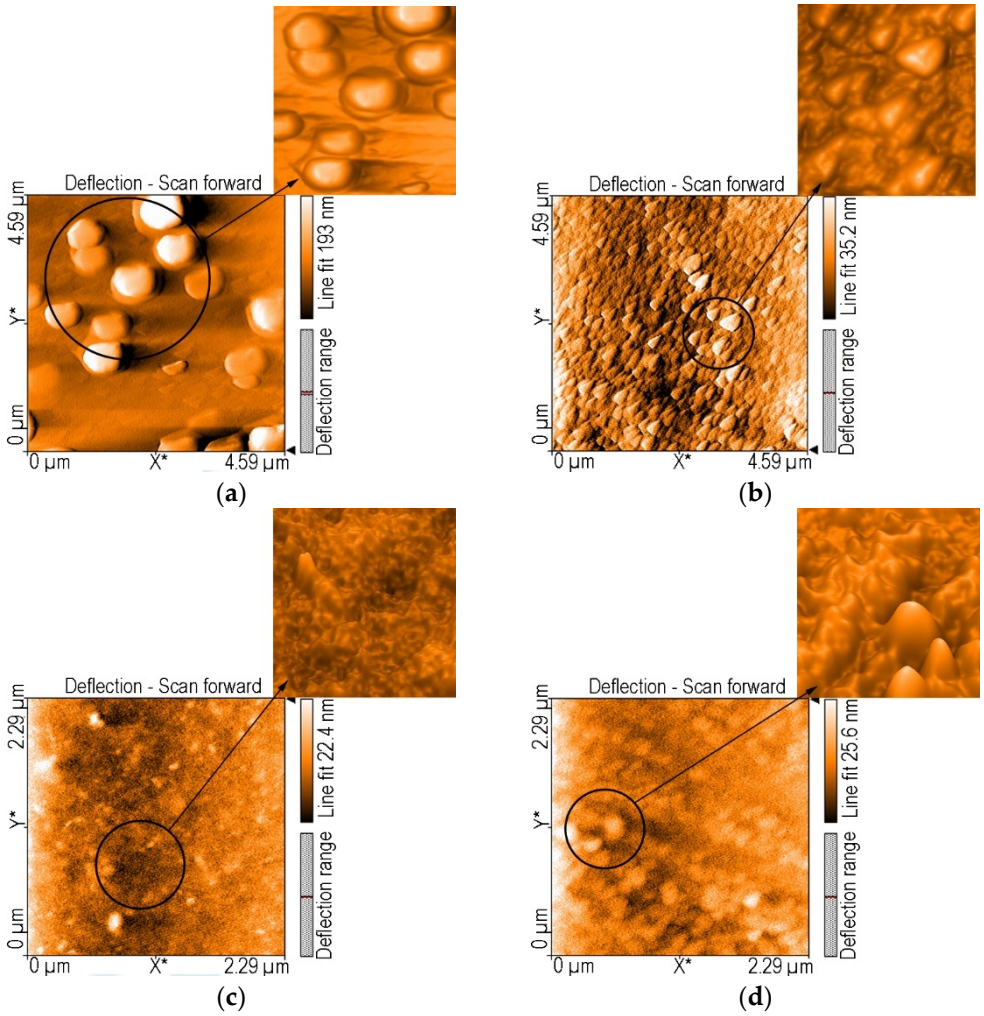


Figure 8. The 2D and 3D AFM images of (5-COOCH3-3MPP) deposited from THF (**a**); (5-COOH-3MPP) deposited from THF (**b**); (5-COOH-3MPP)-k-carrageenan composite material deposited from DMF-water mixture (**c**); (5-COOH-3MPP)-k-carrageenan composite material after capturing CO_2 gas, in liquid DMF-water mixture (**d**).

The 4 µm × 4 µm 2D AFM image of 5-(4-carboxy-phenyl)-10,15,20-tris-(4-methyl-phenyl)-porphyrin deposited from THF (Figure 8b) reveals both H- and J-type aggregated triangle-shaped architectures with similar sizes and orientation, and distributed on the surface in multiple layers. This kind of morphology was found in our studies [29–32].

The composite material (5-COOH-3MPP)-k-carrageenan deposited from DMF-water mixture on silica plates (Figure 8c) reveals an uneven porous surface, having isolated aggregates with particle height distribution 6.70–13.2 nm.

After treatment with CO_2 gas, the AFM images of 5-COOH-3MPP-k-carrageenan composite material (Figure 8d) presents a considerably modified height distribution of particles, from 9.4 to 14.8 nm, consistent with the hypothesis of incorporating CO_2 gas in

the gel. The aggregates are larger and distributed like parallel rows on the surface. It is clear that a reconfiguration of the porphyrin–polymer surface has occurred.

3.2. Method for Obtaining (5-COOH-3MPP)-k-Carrageenan-AuNPs Hybrid Material

Gold colloidal solution was prepared by adapting a previously reported method [33,34], from $HAuCl_4 \cdot 3H_2O$ and sodium citrate. The final content in AuNPs in the colloid was 6.91×10^{-4} M.

The complex of the porphyrin-k-carrageenan and AuNPs was obtained as follows: 1.76 mL (5-COOH-3MPP)-k-carrageenan gel was diluted with 28.24 mL DMF, acidified with HCl (c = 37%), in which a drastic change in color from pink to green took place. Then, portions of 0.2 mL concentrated gold colloid solution were added. The mixture was stirred for 90 s and the UV-Vis spectra were recorded after each adding (Figure 9). The color changed from green to dark blue, making this material suitable as colorimetric sensor for gold nanoparticles. This material can serve as optical sensitive material for AuNPs detection (Figure S9-Supplementary Material).

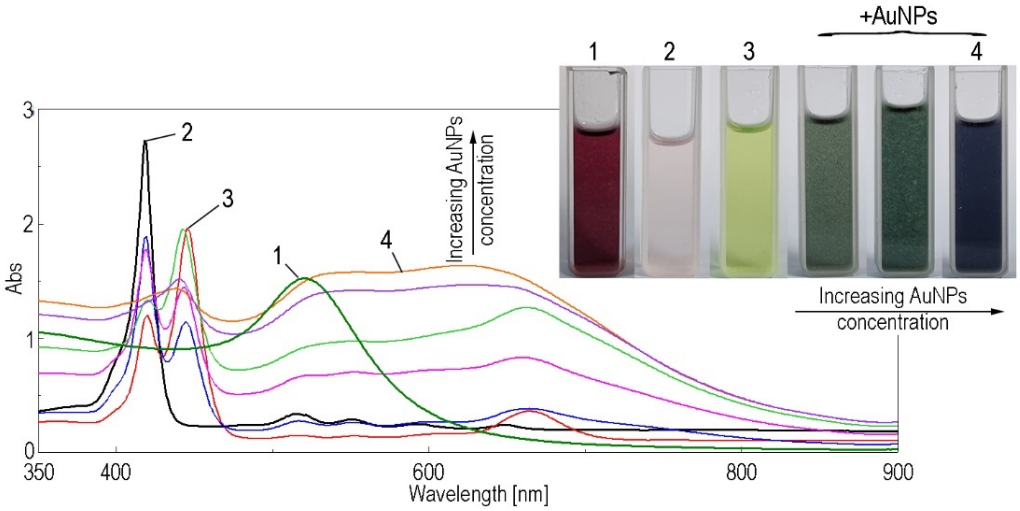


Figure 9. Overlapped UV-Vis spectra: gold colloid (1); (5-COOH-3MPP)-k-carrageenan composite material (2); acidified porphyrin-k-carrageenan composite material showing the diprotonated form of porphyrin (3); 5-COOH-3MPP porphyrin-k-carrageenan-AuNPs material (4).

It can be observed that the adding of colloidal gold significantly increases the intensity of the bands located at 520 nm. Simultaneously, a considerable enlargement of the absorption domain is obtained from 500 nm up to 680 nm, generating a plasmonic plateau. The Soret band originating from the (5-COOH-3MPP) porphyrin is red shifted toward 460 nm (due to J type aggregates generation), then blue shifted to 450 nm due to the plasmonic complex formation. The second absorption peak of the plasmonic plateau, located around 680 nm, is clearly generated by the dramatic hyperchromic transformation of the QI band of the (5-COOH-3MPP) porphyrin during the complex formation with AuNPs.

Based on the synergistic approach between porphyrin-k-carrageenan composite and AuNPs that gave a wide–band absorption material, our aim was to extend its functionality toward ion metal detection from polluted environments and in health monitoring.

3.3. Spectrophotometric Detection of Mn^{2+} Ions by (5-COOH-3MPP)-k-Carrageenan-AuNPs Hybrid Material

The spectroscopic detection of Mn^{2+} ions was performed using the solution of porphyrin-k-carrageenan-AuNPs hybrid material in DMF. To 5 mL solution of (5-COOH-3MPP)-k-carrageenan-AuNPs hybrid material, portions of 0.01 mL $MnCl_2$ solution in water ($c = 1 \times 10^{-3}$ M) are added. The overlapped UV-Vis spectra recorded after each addition of $MnCl_2$ solution, followed by 90 s stirring, are presented in Figure 10.

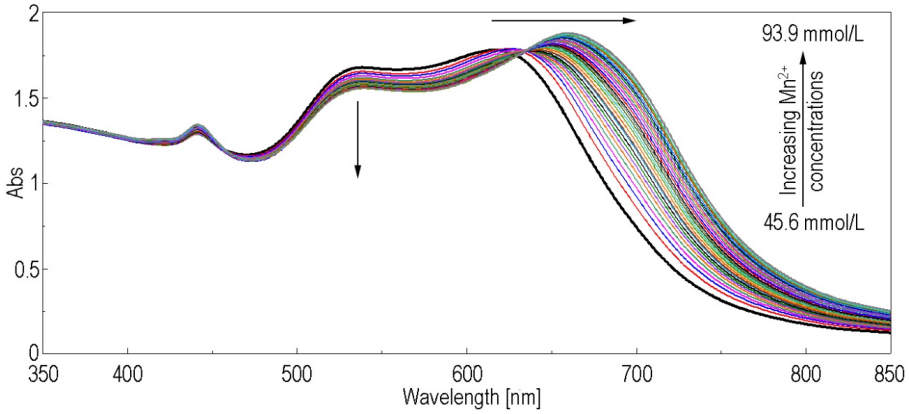


Figure 10. Overlapped UV-Vis spectra for the detection of Mn^{2+} using (5-COOH-3MPP)-k-carrageenan-AuNPs hybrid material, in DMF/water.

As can be observed in Figure 10, adding of the manganese ion changed the aspect of the UV-Vis spectra, consisting first in the constant bathochromic shift of the absorption maximum from 617 nm to 659 nm, accompanied by a constant increase regarding the intensity. The intensity of the band located at 539 nm is constantly increasing in intensity as the Mn^{2+} ion concentration increases. An isosbestic point located at 635 nm indicates that at least one novel intermediate product is formed between Mn^{2+} ions and the porphyrin-base molecule, favored by the AuNPs plasmon. This type of linking manganese ions by porphyrins is based on the multitude of oxidation states in which manganese might exist [29].

The linear dependence between the intensity of the newly formed band at 659 nm and the Mn^{2+} concentration is presented in Figure 11. It is characterized by a very good correlation coefficient of 99.62% for a narrow interval of concentrations from 4.56×10^{-5} M to 9.39×10^{-5} M (5–11 mg/L), which is demanded for the detection of excess manganese in humans exposed to polluted water sources or those who ingested high dietary manganese [18].

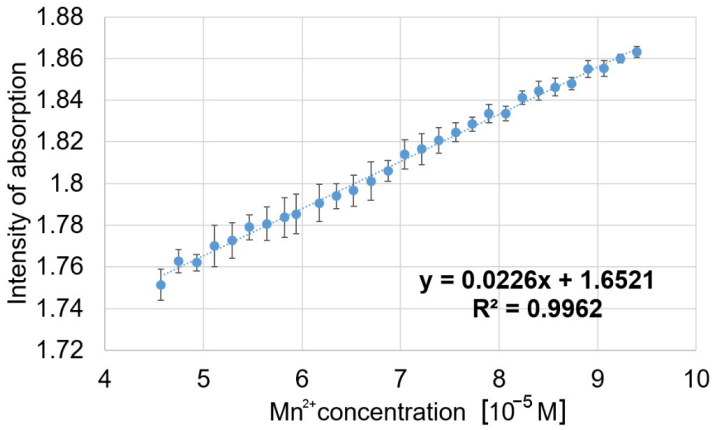


Figure 11. Linear dependence between the intensity of absorption of (5-COOH-3MPP)-k-carrageenan-AuNPs hybrid material measured at 659 nm and the Mn^{2+} ion concentration.

The limit of detection (LOD) for Mn^{2+} is 2.80 μM. It was calculated as LOD = 3.3 σ/S, where σ is the standard deviation of the response and S is the slope of the calibration curve [35].

As a perspective, this plasmonic material might be a suitable sensitive substrate for the design of microsensor devices to medical monitoring of patients suffering from manganism [36].

AFM Investigation of (5-COOH-3MPP)-k-Carrageenan-AuNPs Hybrid Material, before and after Mn^{2+} Detection

AFM images of (5-COOH-3MPP)-k-carrageenan-AuNPs (Figure 12a) show large aggregates grouped in zigzag course, uniformly covered with small round gold particles (<50 nm in diameter). The height distribution of aggregates is 14 to 23 nm.

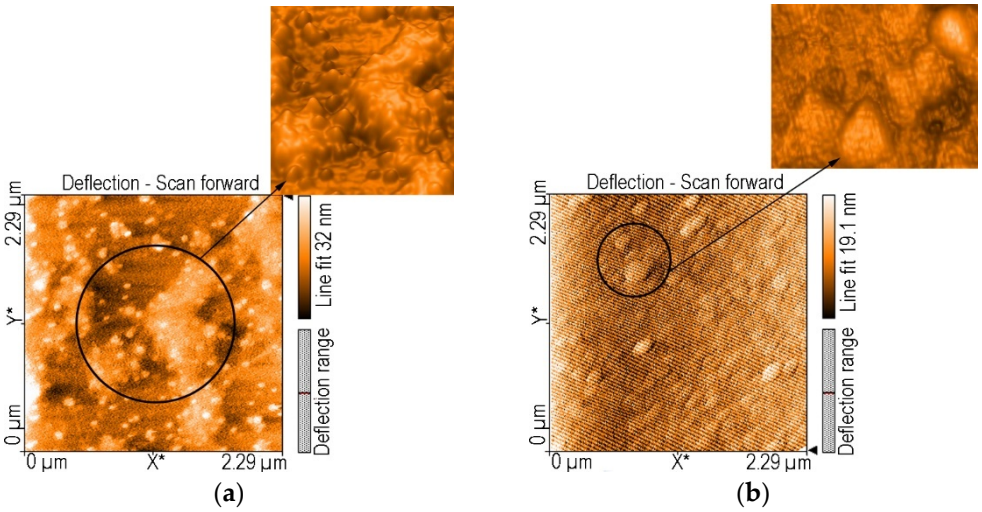


Figure 12. (5-COOH-3MPP)-k-carrageenan-AuNPs hybrid material deposited from DMF-water mixture (**a**); (5-COOH-3MPP)-k-carrageenan-AuNPs hybrid material after Mn^{2+} detection, deposited from DMF-water mixture (**b**).

After interacting with Mn^{2+}, the AFM images of the hybrid material (5-COOH-3MPP)-k-carrageenan-AuNPs (Figure 12b) show small triangular particles, around 200 nm in side, evenly oriented. The J- and H-aggregation processes are amplified, leading to a very adherent, uniform and compact surface.

3.4. Interference Study

In order to verify that the detection of the manganese ion from untreated mine waters is accurate even in the presence of interfering species, the following metallic salts were tested: $CuCl_2$, $FeCl_3$, $FeSO_4$, KCl, NaCl, $ZnCl_2$, $Pb(NO_3)_2$, $MgSO_4$ and $CaCl_2$.

A solution of porphyrin-k-carrageenan-AuNPs hybrid material containing Mn^{2+} with a concentration of 4.5×10^{-5} M was prepared. The reference sample was composed from 2 mL of this solution in which 0.1 mL distilled water was added to replace any false results due to dilution. Portions of 0.1 mL containing each of the tested interferent, to provide a final concentration of interfering species 1000 times higher than that of Mn^{2+}, have been introduced to the 2 mL samples already containing Mn^{2+}. The UV-Vis spectra were recorded for each interferent and superposed in (Figure S10-Supplementary Material).

Average percentage errors calculation is: $|\Delta I/I| \times 100$, where I represents the absorption intensity of the sample containing only Mn^{2+} and ΔI the difference between I and the absorption intensity of the samples containing Mn^{2+} mixed with each studied interfering analyte. From Figure 13 it can be observed that only Mg^{2+} and Ca^{2+} ions slightly interfere in the Mn^{2+} detection, introducing in the analysis an average percentage error between 3.50–3.90.

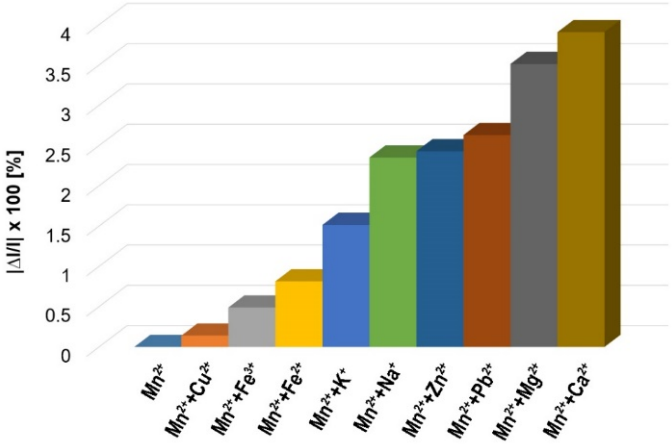


Figure 13. The graphical representation of the average percentage errors produced by several interfering ions in the detection of Mn^{2+}.

We can conclude that there is a good selectivity of the detection for Mn^{2+} in the presence of interfering cations.

4. Conclusions

Two A_3B-type porphyrins were synthesized and characterized by UV-Vis, FT-IR, NMR and AFM spectroscopy, namely: 5-(4-methoxy-carbonyl-phenyl)-10,15,20-tris-(4-methyl-phenyl)-porphyrin and 5-(4-carboxyphenyl)-10,15,20-tris-(4-methyl-phenyl)-porphyrin. The carboxyl-substituted derivative was coupled with k-carrageenan in order to obtain a composite and was able to capture CO_2. The composite material (1 g) can capture 6.97 mmol CO_2. This result is among the best performances reported till now [2,5,9], presenting the advantage of acting under normal conditions.

The optical properties of the porphyrin-k-carrageenan composite material were improved by complexing it with AuNPs, when the obtained wide plasmonic plateau (520–680 nm) display also a significant hyperchromic effect. As a result of this experiment, a large concentration domain of AuNPs, from 4×10^{-6} M to 4×10^{-4} M, can be optically detected with high confidence and might be useful for the monitoring of gold nanoparticles in fibroblasts.

The porphyrin-k-carrageenan-AuNPs complex nanomaterial was able to detect Mn^{2+} ions in solution with high precision in the concentration interval of 4.56×10^{-5} M to 9.39×10^{-5} M (5–11 mg/L) that can be practical in the detection of excess manganese in polluted water sources or in humans that ingested toxic levels of dietary manganese. The accuracy of the Mn^{2+} detection was verified by adding interfering metallic salts: $CuCl_2$, $FeCl_3$, $FeSO_4$, KCl, NaCl, $ZnCl_2$, $Pb(NO_3)_2$, $MgSO_4$ and $CaCl_2$ at concentrations 1000 times higher than that of Mn^{2+}. The conclusion was that only Mg^{2+} and Ca^{2+} ions slightly interfere in the Mn^{2+} detection, introducing in the analysis an average percentage error between 3.50–3.90.

In conclusion, the partnership between 5-(4-carboxyphenyl)-10,15,20-tris-(4-methyl-phenyl)-porphyrin, k-carrageenan and AuNPs can generate multifunctional materials acting as gas sorbents or sensitive materials for toxic metal ion detection with relevance in environmental and medical monitoring and rehabilitation.

Supplementary Materials: The following supporting information can be downloaded at: https://www.mdpi.com/article/10.3390/chemosensors10040133/s1, Figure S1. The multicomponent synthesis of 5-(4-methoxycarbonyl-phenyl)-10,15,20-tris-(4-methyl-phenyl)-porphyrin and the mixture of six resulted porphyrins; Figure S2. The TLC plate presenting the four separated compounds from the multicomponent synthesis of 5-(4-methoxycarbonyl-phenyl)-10,15,20-tris-(4-methyl-phenyl)-porphyrin, eluted with CH_2Cl_2; Figure S3. Superposed UV-Vis spectra of (5-COOCH3-3MPP) and (5-COOH-3MPP) in THF, both solutions of equal concentration, c = 4.095×10^{-6} M, 1 cm opti-

cal path length, scan speed of 1000 nm/min and blank line was obtained in bare THF; Figure S4. Overlapped FT-IR spectra of (5-COOCH3-3MPP) and (5-COOH-3MPP) in KBr pellets; Figure S5. ^{1}H-NMR spectrum of (5-COOCH3-3MPP)porphyrin in $CDCl_3$; Figure S6. ^{13}C-NMR spectrum of 5-(4-methoxycarbonyl-phenyl)-10,15,20-tris-(4-methyl-phenyl)-porphyrin; Figure S7. ^{1}H-NMR spectrum of (5-COOH-3MPP) porphyrin in $CDCl_3$; Figure S8. The installation for the capturing of CO_2 gas by the porphyrin-k-carrageenan composite material; Figure S9. Linear dependence between the intensity of absorption of 5-COOH-3MPP porphyrin-k-carrageenan material measured at 520 nm and the AuNPs concentration; Figure S10. Overlapped UV-Vis spectra for the reference and for the presence of each interfering metallic salt: $CuCl_2$, $FeCl_3$, $FeSO_4$, KCl, NaCl, $ZnCl_2$, $Pb(NO_3)_2$, $MgSO_4$, $CaCl_2$. References [37–47] are cited in the Supplementary Materials.

Author Contributions: C.E. and I.F. contributed equally to this work. Conceptualization, E.F.-C.; methodology, E.F.-C., C.E. and I.F.; software, I.F. and A.-M.M.; validation, E.F.-C.; formal analysis, A.-M.M., C.E., I.F., A.L., C.I. and M.B.; investigation, C.E., I.F., A.L., C.I., M.B. and A.-M.M.; resources, E.F.-C.; data curation, C.E., I.F., A.-M.M. and C.I.; writing—original draft preparation, I.F. and C.E.; writing—review and editing, E.F.-C.; visualization, E.F.-C.; supervision, E.F.-C.; project administration, E.F.-C. and M.B.; funding acquisition, E.F.-C. All authors have read and agreed to the published version of the manuscript.

Funding: This research was funded by UEFISCDI, project number PN-III-P2-2.1-PED-2019-0487, 528PED/2020, CeraPor-Corr -"Hybrid ceramics/porphyrins, deposited by pulsed laser deposition as single and sandwich layers for corrosion inhibition of steels in acid environment" and partially by Romanian Academy through Programme 3/2022 from the Institute of Chemistry "Coriolan Dragulescu".

Institutional Review Board Statement: Not applicable.

Informed Consent Statement: Not applicable.

Data Availability Statement: Not applicable.

Conflicts of Interest: All authors declare that the research was conducted in the absence of any commercial or financial relationships that could be construed as a potential conflict of interest.

References

1. Zhang, L.; Feng, Y.; He, H.; Liu, Y.; Weng, J.; Zhang, P.; Huang, W. Construction of hexanuclear Ce(III) metal−porphyrin frameworks through linker induce strategy for CO_2 capture and conversion. *Catal. Today* **2021**, *374*, 38–43. [CrossRef]
2. Chang, S.; Xie, W.; Yao, C.; Xu, G.; Zhang, S.; Xu, Y.; Ding, X. Construction of 2D porphyrin-based covalent organic framework as adsorbent for organic dyes removal and carbon dioxide adsorption. *J. Solid State Chem.* **2021**, *304*, 122577. [CrossRef]
3. Chi, H.; Chen, H.; Gong, K.; Wang, X.; Zhang, Y. Protein-caged zinc porphyrin as a carbonic anhydrase mimic for carbon dioxide capture. *Sci. Rep.* **2020**, *10*, 19581. [CrossRef] [PubMed]
4. Radford, S.E. GroEL: More than Just a Folding Cage. *Cell* **2006**, *125*, 831–833. [CrossRef] [PubMed]
5. Li, Y.; Zhang, J.; Zuo, K.; Li, Z.; Wang, Y.; Hu, H.; Zeng, C.; Xu, H.; Wang, B.; Gao, Y. Covalent Organic Frameworks for Simultaneous CO2 Capture and Selective Catalytic Transformation. *Catalysts* **2021**, *11*, 1133. [CrossRef]
6. Kaplan, E.; Gümrükçü, S.; Gençten, M.; Şahin, Y.; Hamuryudan, E. Thiophene Functionalized Porphyrin for Electrochemical Carbon Dioxide Reduction. *J. Electrochem. Soc.* **2021**, *168*, 126512. [CrossRef]
7. Mak, C.A.; Pericas, M.A.; Fagadar-Cosma, E. Functionalization of A3B-type porphyrin with Fe_3O_4 MNPs. Supramolecular assemblies, gas sensor and catalytic applications. *Catal. Today* **2018**, *306*, 268–275. [CrossRef]
8. Anghel, D.; Lascu, A.; Epuran, C.; Fratilescu, I.; Ianasi, C.; Birdeanu, M.; Fagadar-Cosma, E. Hybrid Materials Based on Silica Matrices Impregnated with Pt-Porphyrin or PtNPs Destined for CO_2 Gas Detection or for Wastewaters Color Removal. *Int. J. Mol. Sci.* **2020**, *21*, 4262. [CrossRef]
9. Liu, J.; Fan, Y.Z.; Li, X.; Xu, Y.W.; Zhang, L.; Su, C.Y. Catalytic Space Engineering of Porphyrin Metal-Organic Frameworks for Combined CO_2 Capture and Conversion at a Low Concentration. *ChemSusChem* **2018**, *11*, 2340–2347. [CrossRef]
10. Fagadar-Cosma, E.; Vlascici, D.; Fagadar-Cosma, G.; Palade, A.; Lascu, A.; Creanga, I.; Birdeanu, M.; Cristescu, R.; Cernica, I. A Sensitive A_3B Porphyrin Nanomaterial for CO_2 Detection. *Molecules* **2014**, *19*, 21239–21252. [CrossRef]
11. Fagadar-Cosma, E.; Tarabukina, E.; Zakharova, N.; Birdeanu, M.; Taranu, B.; Palade, A.; Creanga, I.; Lascu, A.; Fagadar-Cosma, G. Hybrids formed between polyvinylpyrrolidone and an A_3B porphyrin dye: Behavior in aqueous solutions and chemical response to CO_2 presence. *Polym. Int.* **2016**, *65*, 200–209. [CrossRef]
12. Liu, Z.; Gao, T.; Yang, Y.; Meng, F.; Zhan, F.; Jiang, Q.; Sun, X. Anti-Cancer Activity of Porphyran and Carrageenan from Red Seaweeds. *Molecules* **2019**, *24*, 4286. [CrossRef] [PubMed]

13. Shang, Q.; Sun, W.; Shan, X.; Jiang, H.; Yu, G. Carrageenan-induced colitis is associated with decreased population of anti-inflammatory bacterium, Akkermansia muciniphila, in the gut microbiota of C57BL/6J mice. *Toxicol. Lett.* **2017**, *279*, 87–95. [CrossRef] [PubMed]
14. Hipolito Júnior, E.; Gonçalves, A.G.; Noseda, M.D.; Duarte, M.E.R.; Murakami, F.S.; Ducatti, D.R.B. Semi-synthesis of N-alkyl-kappa-carrageenan derivatives and evaluation of their antibacterial activity. *Carbohydr. Res.* **2021**, *499*, 108234. [CrossRef]
15. Larotonda, F.D.S.; Torres, M.D.; Gonçalves, M.P.; Sereno, A.M.; Hilliou, L. Hybrid carrageenan-based formulations for edible film preparation: Benchmarking with kappa carrageenan. *J. Appl. Polym. Sci.* **2015**, *133*, 42263. [CrossRef]
16. Sepúlveda, M.R.; Dresselaers, T.; Vangheluwe, P.; Everaerts, W.; Himmelreich, U.; Mata, A.M.; Wuytack, F. Evaluation of manganese uptake and toxicity in mouse brain during continuous $MnCl_2$ administration using osmotic pumps. *Contrast Media Mol. Imaging* **2012**, *7*, 426–434. [CrossRef]
17. Li, Y.; Xu, Z.; Ma, H.; Hursthouse, A.S. Removal of Manganese(II) from Acid Mine Wastewater: A Review of the Challenges and Opportunities with Special Emphasis on Mn-Oxidizing Bacteria and Microalgae. *Water* **2019**, *11*, 2493. [CrossRef]
18. Du, J. Drinking Water Health Advisory for Manganese in: United States Environmental Protection Agency: Prepared by: U.S. Environmental Protection Agency Office of Water (4304T). 2004. Available online: https://www.epa.gov/sites/default/files/2014-09/documents/support_cc1_magnese_dwreport_0.pdf (accessed on 15 February 2022).
19. O'Neal, S.L.; Zheng, W. Manganese Toxicity Upon Overexposure: A Decade in Review. *Curr. Environ. Health Rep.* **2015**, *2*, 315–328. [CrossRef]
20. Klemnmann, R.L.P.; Watzlar, G.R. Should the efluent limits for manganese be modified? In *Mine Drainage and Surface Mine Reclamation, Volume II: Mine Reclamation, Abandoned Mine Lands and Policy Issues, Proceedings of the Annual meeting of the American Society for Surface Mining and Reclamation, Pittsburgh, PA, USA, 17 April 1988*; Brown, D.S., Ed.; Department of the Interior, Bureau of Mines: Washington, DC, USA, 1988; pp. 305–310.
21. Fuchida, S.; Tajima, S.; Nishimura, T.; Tokoro, C. Kinetic Modeling and Mechanisms of Manganese Removal from Alkaline Mine Water Using a Pilot Scale Column Reactor. *Minerals* **2022**, *12*, 99. [CrossRef]
22. Palade, A.; Fagadar-Cosma, G.; Lascu, A.; Creanga, I.; Birdeanu, M.; Fagadar-Cosma, E. New porphyrin-based spectrophotometric sensor for Ag^0 detection. *Dig. J. Nanomater. Bios* **2013**, *8*, 1013–1022.
23. Anghel, D.; Birdeanu, M.; Lascu, A.; Epuran, C.; Fagadar-Cosma, E. Amino-substituted porphyrins at the border of hybrid materials generation and platinum nanoparticles detection. *Studia Univ. Babes-Bolyai Chem.* **2020**, *2*, 107–120. [CrossRef]
24. Ţaranu, B.O.; Vlascici, D.; Sebarchievici, I.; Fagadar-Cosma, E. The aggregation behavior of an A_3B free base porphyrin and its application as chromium(III)-selective membrane sensor. *Studia Univ. Babes-Bolyai Chem.* **2016**, *61*, 199–212.
25. Vlascici, D.; Popa, I.; Chiriac, V.A.; Fagadar-Cosma, G.; Popovici, H.; Fagadar-Cosma, E. Potentiometric detection and removal of copper using porphyrins. *Chem. Cent. J.* **2013**, *7*, 111. [CrossRef] [PubMed]
26. Vlascici, D.; Fagadar-Cosma, E.; Popa, I.; Chiriac, V.; Gil-Agusti, M. A Novel Sensor for Monitoring of Iron(III) Ions Based on Porphyrins. *Sensors* **2012**, *12*, 8193–8203. [CrossRef] [PubMed]
27. Wang, F.; Chen, L.; Zhu, J.; Hu, X.; Yang, Y. A Phosphorescence Quenching-Based Intelligent Dissolved Oxygen Sensor on an Optofluidic Platform. *Micromachines* **2021**, *12*, 281. [CrossRef]
28. Fratilescu, I.; Dudás, Z.; Birdeanu, M.; Epuran, C.; Anghel, D.; Fringu, I.; Lascu, A.; Len, A.; Fagadar-Cosma, E. Hybrid silica materials applied for fuchsine B color removal from wastewaters. *Nanomaterials* **2021**, *11*, 863. [CrossRef] [PubMed]
29. Sebarchievici, I.; Lascu, A.; Fagadar-Cosma, G.; Palade, A.; Fringu, I.; Birdeanu, M.; Taranu, B.; Fagadar-Cosma, E. Optical and electrochemical mediated detection of ascorbic acid using manganese porphyrin and its gold hybrids. *Comptes Rendus Chim.* **2018**, *21*, 327–338. [CrossRef]
30. Salageanu, L.; Lascu, A.; Birdeanu, M.; Fagadar-Cosma, E. Plasmonic Material Based on Silver Colloid and Zn-Metalloporphyrin for Drug Detection of p-Aminosalicylic Acid. *Dig. J. Nanomater. Biostructures* **2018**, *13*, 653–659.
31. Lascu, A.; Palade, A.; Birdeanu, M.; Fagadar-Cosma, E. Procaine detection using hybrids of cobalt-metalloporphyrin with gold and silver nanoparticles. *J. Chem. Soc. Pak.* **2019**, *41*, 43–51.
32. Lascu, A.; Birdeanu, M.; Taranu, B.; Fagadar-Cosma, E. Hybrid Mn-Porphyrin-Nano Gold Nanomaterial Applied for the Spectrophotometric Detection of β-Carotene. *J. Chem.* **2018**, *2018*, 5323561. [CrossRef]
33. Muthukumar, P.; Abraham John, S. Gold nanoparticles decorated on cobalt porphyrin-modified glassy carbon electrode for the sensitive determination of nitrite ion. *J. Colloid Interface Sci.* **2014**, *421*, 78–84. [CrossRef] [PubMed]
34. Fagadar-Cosma, E.; Lascu, A.; Shova, S.; Zaltariov, M.F.; Birdeanu, M.; Croitor, L.; Balan, A.; Anghel, D.; Stamatin, S. X-ray structure elucidation of a Pt-metalloporphyrin and its application for obtaining sensitive AuNPs-plasmonic hybrids capable to detect triiodide anions. *Int. J. Mol. Sci.* **2019**, *20*, 710. [CrossRef] [PubMed]
35. Desmoni, E.; Brunetti, B. About Estimating the Limit of Detection by the Signal to Noise Approach. *Pharm. Anal. Acta* **2015**, *6*, 1000355. [CrossRef]
36. Wang, F.; Zhu, J.; Hu, X.; Chen, L.; Zuo, Y.; Yang, Y.; Jiang, F.; Sun, C.; Zhao, W.; Han, X. Rapid nitrate determination with a portable lab-on-chip device based on double microstructured assisted reactors. *Lab Chip* **2021**, *21*, 1109–1117. [CrossRef]
37. Bakar, M.B.; Oelgemöller, M.; Senge, M.O. Lead structures for applications in photodynamic therapy. Part 2: Synthetic studies for photo-triggered release systems of bioconjugate porphyrin photosensitizers. *Tetrahedron* **2009**, *65*, 7064–7078. [CrossRef]

38. Scalise, I.; Durantini, E.N. Synthesis and photodynamic activity of metallo 5-(4-carboxyphenyl)-10,15,20-tris(4-methylphenyl) porphyrins. In Proceedings of the Sixth International Electronic Conference on Synthetic Organic Chemistry (ECSOC-6), Internet, 1–30 September 2002; Available online: https://www.mdpi.org/ecsoc/ecsoc-6/Papers/C007/C007.htm (accessed on 15 February 2022).
39. Fagadar-Cosma, E.; Vlascici, D.; Birdeanu, M.; Fagadar-Cosma, G. Novel fluorescent pH sensor based on 5-(4-carboxy-phenyl)-10,15,20-tris(phenyl)-porphyrin. *Arab. J. Chem.* **2019**, *12*, 1587–1594. [CrossRef]
40. Max, J.J.; Chapados, C. Infrared Spectroscopy of Aqueous Carboxylic Acids: Comparison between Different Acids and Their Salts. *J. Phys. Chem. A* **2004**, *108*, 3324–3337. [CrossRef]
41. Sanches, N.B.; Pedro, R.; Diniz, M.F.; Mattos ED, C.; Cassu, S.N.; Dutra, R.D.C.L. Infrared Spectroscopy Applied to Materials Used as Thermal Insulation and Coatings. *J. Aerosp. Technol. Manag.* **2013**, *5*, 421–430. [CrossRef]
42. Mishra, M.K. Fourier Transform Infrared Spectrophotometry Studies of Chromium Trioxide-Phthalic Acid Complexes. *Chem. Sci. Trans.* **2016**, *5*, 770–774. [CrossRef]
43. Pangajavalli, S.; Ranjithkumar, R.; Sridhar, B.; Ramaswamy, S. Hirshfeld and Vibrational Analysis of 5-Benzyl-7a-Hydroxy-1-Methyl-2,3,5,6,7,7a-Hexahydro-1H-3a, 7-Methanoindeno [2,1-d]Pyrrolo[3,2-c]Azepine-12,13(4H)-Dione. *MMSE* **2017**. [CrossRef]
44. Coates, J. Interpretation of Infrared Spectra, A Practical Approach. In *Encyclopedia of Analytical Chemistry*; Meyers, R.A., Ed.; John Wiley & Sons Ltd.: Chichester, UK, 2000; pp. 10815–10837.
45. Falagan-Lotsch, P.; Grzincic, E.M.; Murphy, C.J. One low-dose exposure of gold nanoparticles induces long-term changes in human cells. *Proc. Natl. Acad. Sci. USA* **2016**, *113*, 13318–13323. [CrossRef] [PubMed]
46. Sani, A.; Cao, C.; Cui, D. Toxicity of gold nanoparticles (AuNPs): A review. *Biochem. Biophys. Rep.* **2021**, *26*, 100991. [CrossRef] [PubMed]
47. Coradeghini, R.; Gioria, S.; García, C.P.; Nativo, P.; Franchini, F.; Gilliland, D.; Ponti, J.; Rossi, F. Size-dependent toxicity and cell interaction mechanisms of gold nanoparticles on mouse fibroblasts. *Toxicol. Lett.* **2013**, *217*, 205–216. [CrossRef] [PubMed]